Earth and Planetary Science Letters 357–358 (2012) 194–202

Contents lists available at SciVerse ScienceDirect

Earth and Planetary Science Letters

journal homepage: www.elsevier.com/locate/epsl

Discussion

Synthesis and equation of state of perovskites in the $(Mg, Fe)_3Al_2Si_3O_{12}$ system to 177 GPa

Susannah M. Dorfman [a,*], Sean R. Shieh [b], Yue Meng [c], Vitali B. Prakapenka [d], Thomas S. Duffy [a]

[a] Department of Geosciences, Princeton University, Princeton, NJ 08544, USA
[b] Department of Earth Sciences, The University of Western Ontario, London, Ontario, Canada N6A 5B7
[c] High-Pressure Collaborative Access Team, Carnegie Institution of Washington, 9700 South Cass Avenue, Argonne, IL 60439, USA
[d] Center for Advanced Radiation Sources, The University of Chicago, 9700 South Cass Avenue, Argonne, IL 60439, USA

ARTICLE INFO

Article history:
Received 16 February 2012
Received in revised form
20 August 2012
Accepted 17 September 2012
Editor: L. Stixrude

Keywords:
perovskite
post-perovskite
lower mantle
D″ region

ABSTRACT

Natural and synthetic pyrope–almandine compositions from 38 to 100 mol% almandine (Alm38–Alm100) were studied by synchrotron X-ray diffraction in the laser-heated diamond anvil cell to 177 GPa. Single-phase orthorhombic $GdFeO_3$-type perovskites were synthesized across the entire examined compositional range at deep lower mantle pressures, with higher Fe-contents requiring higher synthesis pressures. The formation of perovskite with Alm100 ($Fe_3Al_2Si_3O_{12}$) composition at 80 GPa marks the first observation of a silicate perovskite in a Fe end-member. Fe-enrichment broadens and lowers the pressure range of the post-perovskite transition for intermediate compositions such as Alm54, but the more Fe-rich Alm100-composition perovskite remains stable to pressures as high as 149 GPa. Volume compression data for the Alm54 and Alm100 compositions were fit to the Birch–Murnaghan equation of state. The compressibility of perovskites synthesized from compositions along the pyrope–almandine join is not strongly sensitive to Fe-content. The compression curves were smooth over the entire measured range, and no evidence for a volume anomaly associated with a spin transition was observed.

In the Earth's deep lower mantle, seismic imaging has identified regions of high density and low shear wave speed as possible thermochemical piles (Garnero and McNamara, 2008). These large low shear velocity provinces (LLSVPs) on the scale of ~1000 km (Ishii and Tromp, 2004; Trampert et al., 2004) may be sequestered primitive mantle (Lee et al., 2010) or stagnating Fe,Al-rich subducted slabs (Williams and Garnero, 1996; McNamara and Zhong, 2005). In order to evaluate which hypotheses match geophysical constraints on the properties of the LLSVPs, this study explores how variations in Fe and Al content affect stability and observable physical properties of silicates stable under deep mantle conditions.

Garnet is the major Al-bearing mineral of the upper mantle and transition zone and a useful starting material for investigating the incorporation of Fe and Al in lower mantle silicates (Kesson et al., 1995). At 37–40 GPa, pyrope ($Mg_3Al_2Si_3O_{12}$) garnet transforms to the dominant phase of the lower mantle, orthorhombic (Mg, Al)(Al, Si)O_3 perovskite ($GdFeO_3$-type, *Pbnm*, Z=4) (Liu, 1974; Irifune et al., 1996; Ito et al., 1998; Kubo and Akaogi, 2000). Almandine ($Fe_3Al_2Si_3O_{12}$) garnet, however, has not been observed to form perovskite; it breaks down to a mixture of stishovite, wüstite, and corundum at 20–21 GPa and 1200–1600 °C (Conrad et al., 1996; Akaogi et al., 1998). In a previous study of the pyrope–almandine (Pyr–Alm) system, samples were heated at 55–70 GPa and examined *ex situ* at ambient pressure and temperature (Kesson et al., 1995). Quench products for compositions up to 75 mol% almandine, Alm75, consisted of rhombohedral perovskites. More Fe-rich compositions including Alm100 were observed to break down to a mixture of perovskite and oxides. This is similar to the reported behavior of compositions in the (Mg, Fe)SiO_3 system; although perovskites with as much as 75% $FeSiO_3$ are stable at deep lower mantle pressures (Tateno et al., 2007; Dorfman et al., in press), perovskite has not been synthesized from $FeSiO_3$, which has instead been observed to dissociate to FeO and SiO_2 from 20 to 150 GPa and ~1800–2100 K (Ming and Bassett, 1975; Mao et al., 2004; Fujino et al., 2009). While the limits of the solubility of Fe and Al components into perovskite have been studied extensively at pressures below 50 GPa (Fei et al., 1996; Mao et al., 1997;

* Corresponding author at: Earth and Planetary Science Laboratory, École Polytechnique Fédérale de Lausanne, CH-1015 Lausanne, Switzerland. Tel.: +41 21 69 33307.
E-mail address: susannah.dorfman@epfl.ch (S.M. Dorfman).

0012-821X/$ - see front matter © 2012 Elsevier B.V. All rights reserved.
http://dx.doi.org/10.1016/j.epsl.2012.09.024

Akaogi et al., 1998; Kubo and Akaogi, 2000; Nishio-Hamane et al., 2005) they are not well-known at deep lower mantle conditions.

Previous findings on the effects of Fe and Al cation substitutions on physical properties of perovskite have been complex and/or inconsistent (Knittle and Jeanloz, 1987; Mao et al., 1991; Andrault, 2001; Andrault et al., 2007; Walter et al., 2004; Lundin et al., 2008; Nishio-Hamane et al., 2008; Catalli et al., 2010, 2011; Fujino et al., 2012; Boffa Ballaran et al., 2012). The different effects of Fe^{2+}, Fe^{3+}, and Al in the perovskite A- and B-sites on the bulk modulus are each controversial: incorporation of ferrous iron has been observed to increase the bulk modulus (Mao et al., 2011; Boffa Ballaran et al., 2012) or have no significant effect (Lundin et al., 2008; Dorfman et al., in press); ferric iron may decrease bulk modulus through a high-to-low electronic spin transition (Catalli et al., 2010, 2011; Fujino et al., 2012) or have no effect (Nishio-Hamane et al., 2008); aluminum may decrease (Zhang and Weidner, 1999; Kubo and Akaogi, 2000; Daniel et al., 2001; Walter et al., 2004; Catalli et al., 2011; Boffa Ballaran et al., 2012), increase (Andrault et al., 2001, 2007) or have no effect (Daniel et al., 2004; Walter et al., 2006) on the bulk modulus. Aluminum may also modify the chemistry and effects of iron incorporation (Fei, 1998; Frost and Langenhorst, 2002; Saikia et al., 2009; Fujino et al., 2012; Boffa Ballaran et al., 2012). However, direct comparison of these previous studies is hampered by differences between experimental conditions including pressure calibrant, calibrant equation of state, and pressure medium. By measuring samples with different compositions under consistent experimental conditions, the effects of Fe and Al on the equation of state and the possible effects of different oxidation states and spin states may become resolvable.

The post-perovskite phase ($CaIrO_3$-type, *Cmcm*, Z=4) observed in $MgSiO_3$ above 125 GPa and 2500 K (Murakami et al., 2004; Oganov and Ono, 2004) has been of much recent interest for its potential to explain seismic observations near the base of the lower mantle. The pressure range at which the post-perovskite transition occurs has been found to be raised, lowered, and/or broadened by changes in composition, depending on Fe and Al content and Fe oxidation state (Shim, 2008). Diamond anvil cell experiments (Mao et al., 2004, 2005, 2006; Tateno et al., 2007) and density functional theory (DFT) calculations (Caracas and Cohen, 2008) have found that ferrous iron stabilizes post-perovskite relative to perovskite and the two-phase mixture is stable over a wide pressure range. In Al-free, Fe^{2+}-rich compositions, post-perovskite has been found to coexist with perovskite at pressures as low as 82 GPa (Tateno et al., 2007; Dorfman et al., in press). However, for the pyrope composition (Fe-free, 25 mol% Al_2O_3), post-perovskite has not been observed below 140 GPa (Tateno et al., 2005). DFT calculations have reported conflicting results for the effect of Al on the transition, some giving a broad two-phase region at higher pressure (Akber-Knutson et al., 2005) and others yield a slightly lower transition pressure and a narrow two-phase interval (Tsuchiya and Tsuchiya, 2008). Paired substitution of ferric iron and Al has been seen to increase the post-perovskite transition pressure (Nishio-Hamane et al., 2007). The combined effect of direct Mg-Fe^{2+} and paired Mg+Si–Al+Al substitutions on the perovskite-post-perovskite transition is not well-constrained.

In this work, we investigate the phase diagram of Pyr–Alm compositions *in situ* to 177 GPa and temperatures as high as 3000 K with X-ray diffraction in the laser-heated diamond anvil cell. We investigate the synthesis conditions for single-phase perovskites and post-perovskites from these compositions. In addition, we examine the breakdown of Fe^{2+}, Al-rich perovskites at lower pressures and the perovskite-post-perovskite transition at higher pressures. We measure the equations of state of perovskites synthesized from Alm54 and Alm100 compositions under consistent experimental conditions as those in our previous work on Al-free compositions (Dorfman et al., in press).

1. Method

Fe-bearing samples with compositions close to the Pyr–Alm join were selected for study. These are the same materials used in the recent work by Shieh et al. (2011). Compositions were determined by electron microprobe analysis and are listed in Shieh et al. (2011). Microprobe analyses (Hofmeister, 2006) and energy-resolved Mössbauer spectroscopy indicated no detectable ferric iron in the starting materials. Samples with Fe# (Fe/(Fe+Mg+Ca+Mn) in mol%) 38, 54, and 73 (Alm38, Alm54 and Alm73) are natural samples containing minor amounts of Ca and Mn (Hofmeister et al., 1998; Hofmeister, 2006) while Fe# 90 and 100 materials (Alm90 and Alm100) are pure synthetic glasses. The Alm90 glass is richer in Al_2O_3 content than an ideal almandine by $\sim$5 mol%.

Samples were ground into powders and mixed with 15 wt% Au powder as an internal pressure calibrant (Fei et al., 2007). Compacted powder mixtures were either sandwiched between NaCl or supported by NaCl and loaded in Ne as quasi-hydrostatic pressure medium. NaCl was kept in an oven at 110 °C until immediately prior to loading. Samples were loaded in holes drilled through Re gaskets preindented to 20−35 μm thickness. Symmetric piston-cylinder diamond anvil cells with either flat anvils of 200 μm diameter or beveled culets with inner diameters of 100 or 75 μm were used to generate pressures up to 177 GPa. Errors in pressure due to uncertainty in the calibrant lattice parameter and effects of differential stress are estimated to be 1–2 GPa for annealed samples.

Angle-dispersive X-ray diffraction with *in situ* laser heating was performed at beamlines 13-ID-D of the GSECARS sector and 16-ID-B of the HPCAT sector of the Advanced Photon Source (APS). At both facilities the X-ray beam was focused with a Kirkpatrick–Baez double mirror system to dimensions between 3–5×4−10 μm. Diffraction patterns were collected using a MarCCD detector. The position and orientation of the detector were calibrated using a CeO_2 standard. In various experimental runs, X-ray wavelengths were 0.3100–0.4116 Å.

Samples were heated with a Nd:YLF or Nd:YAG double-sided laser heating system (Meng et al., 2006; Prakapenka et al., 2008). Temperatures were measured from both sides by spectroradiometry (Shen et al., 2001). Observed temperatures typically varied by 100 K between upstream and downstream measurements and exhibited 100–400 K variations over 30 min heating times. In a typical synthesis experiment, *in situ* laser heating to 2000–3000 K was carried out for durations of 30–60 min. In addition, we heated to 1500–2000 K for 15–30 min at 5–10 GPa intervals for annealing during equation of state measurements.

Diffraction images were integrated to produce 1-D diffraction patterns using Fit2D software (Hammersley et al., 1996). To obtain peak positions, widths, and intensities, patterns were fit with background-subtracted Voigt lineshapes. Lattice parameters were refined using Unitcell (Holland and Redfern, 1997). Full-profile refinement of selected patterns was conducted using GSAS and EXPGUI software (Larson and Von Dreele, 2000; Toby, 2001).

2. Results

2.1. Heating experiments below 50 GPa

We performed laser heating on Alm100, Alm90, and Alm38 compositions over the range 26–50 GPa. After heating Alm100 glass at 2000 K for 50 min at a starting pressure of 27 GPa, we observed diffraction peaks of stishovite, wüstite, and corundum consistent with the breakdown reaction observed in other studies near 20 GPa (Conrad et al., 1996; Akaogi et al., 1998). No perovskite diffraction peaks were observed. In addition, the

oxides coexist with at least one additional unknown phase up to 35–43 GPa (Supplementary Fig. 1).

An orthorhombic perovskite phase was observed in pyrope–almandine compositions after heating at pressures of 38 GPa and above. During heating of the Alm100 oxide mixture to 2200 K at 42 GPa, the intensities of the oxide peaks weakened as perovskite diffraction peaks grew. A fresh Alm100 sample heated at 43 GPa also formed a mixture of perovskite and oxides, as did Alm90 heated at 39 GPa. By 49 GPa, the dominant phase in the Alm100 sample is perovskite, but weak peaks of the oxide phases persist to at least 58 GPa. These results are inconsistent with Kesson et al. (1995) who reported that no perovskite could be synthesized from Alm100 at 55–70 GPa. For the Alm38 composition, we obtained a mixture of perovskite and oxides after heating at 38 GPa. As pressure increases, the perovskite/oxide ratio increases, and perovskite is the dominant phase at 45 GPa. Even with prolonged heating, it is difficult to completely transform the oxide mixture to single-phase perovskite, likely as a result of slow reaction/diffusion rates.

2.2. Synthesis experiments at 70–90 GPa

In a second set of experiments, the starting materials were compressed directly to 70–90 GPa. Laser heating was carried out to 1600–2530 K at 70–90 GPa for all samples. Prior to heating, diffraction peaks from garnet samples were broad and weak. However, garnet peaks never completely disappeared even upon room-temperature compression to as high as 129 GPa. The transformation from metastable crystalline garnet to perovskite appears to be more sluggish than the transformation from low-Al_2O_3 crystalline starting material such as $(Mg, Fe)_2Si_2O_6$ orthopyroxene. In some runs, broad garnet peaks remained in coexistence with perovskite after stable heating to $\sim$2000 K for 30 or more minutes. No garnet was synthesized in this pressure range when using amorphous starting materials. These slow reaction kinetics have contributed to previous observations of garnet and perovskite coexistence at 50 GPa after laser heating (O'Neill and Jeanloz, 1994).

In experiments on Alm54, Alm90, and Alm100 compositions with stable heating, quenched diffraction patterns showed single-phase orthorhombic $GdFeO_3$-type perovskites (Figs. 1 and 2). We find no evidence for the rhombohedral perovskites reported in the previous work (Kesson et al., 1995). While an Alm90 sample exhibited sharp diffraction peaks after 28 min of heating at 1600–1820 K and 76 GPa, additional time, temperature, and pressure were required to synthesize Alm100 perovskite: best results were achieved with $\sim$60 min heating at 2000–2530 K and above 89 GPa. The Alm100 orthorhombic perovskite structure was indexed by full-profile Rietveld refinement (Fig. 3, Table 1). All peaks were identified as orthorhombic $GdFeO_3$-type perovskite, Au, or NaCl (B2 phase). Lattice parameters, peak shape parameters, and atomic positions were refined for all phases. Atomic positions are similar to values previously obtained for $MgSiO_3$ perovskite (Ross and Hazen, 1990). Preferred orientation was refined for Au and NaCl and was within error of random. Structural parameters derived from full-profile refinement agree with results from peak fitting to 0.1%.

In one experiment, single-phase Alm54 perovskite synthesized at 74 GPa was decompressed directly to 23 GPa without heating. The resulting diffraction pattern showed that broad perovskite diffraction peaks were retained to this pressure (Supplementary Fig. 2). After the sample was then heated to 1100 K for 10 min, the Alm54 perovskite reverted to the garnet structure (Supplementary Fig. 2). Notably, there were no extra or unexplained peaks such as those associated with stishovite. This reversibility of the transformation supports the formation of a single-phase

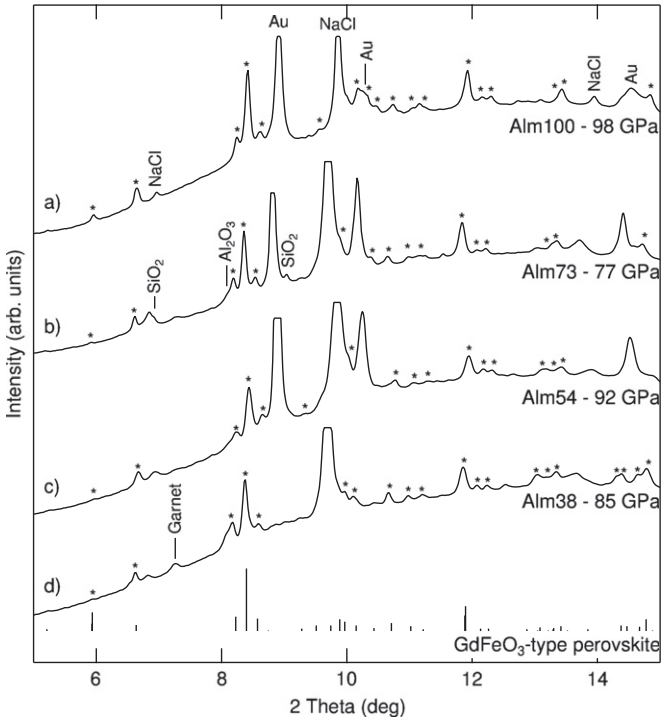

Fig. 1. Representative diffraction patterns ($\lambda = 0.3344$ Å) for orthorhombic $GdFeO_3$-type perovskites synthesized from: (a) Alm100, (b) Alm73, (c) Alm54, and (d) Alm38. All unlabeled peaks can be indexed to reference stick pattern for $GdFeO_3$-type perovskite. For Alm73 and Alm38 compositions, perovskite peaks are accompanied by minor SiO_2, Al_2O_3, and untransformed garnet.

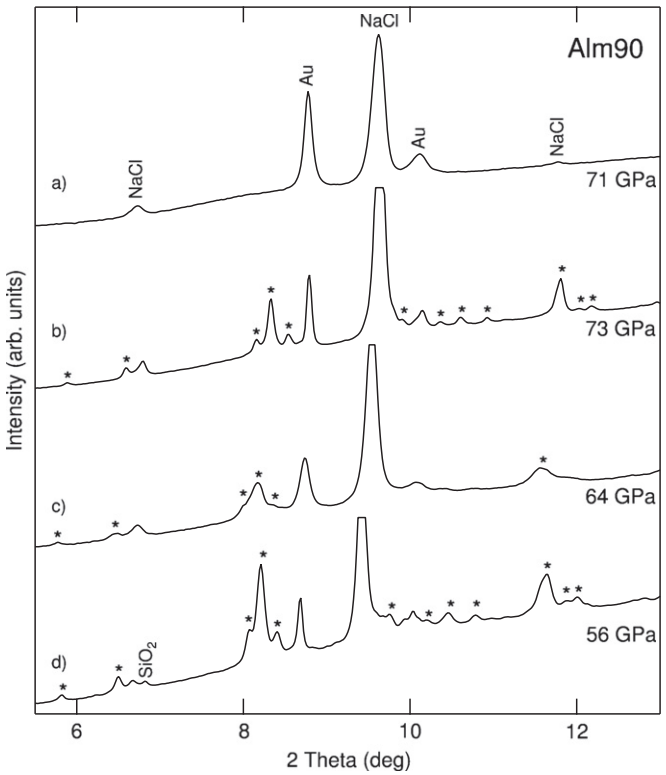

Fig. 2. Representative diffraction patterns ($\lambda = 0.3344$ Å) for Alm90 (asterisks = perovskite peaks): (a) before heating at 71 GPa, (b) after heating, (c) decompressed to 64 GPa, and (d) after heating at 56 GPa. Full width at half maximum (FWHM) measured for Au (111) near 9° and perovskite triplet (020), (112), (200) near 8° decreased $\sim$40% from (a) to (b) and 25–60% from (c) to (d) due to annealing of microstrain during heating and increased 50–100% from (b) to (c) due to strain buildup during decompression.

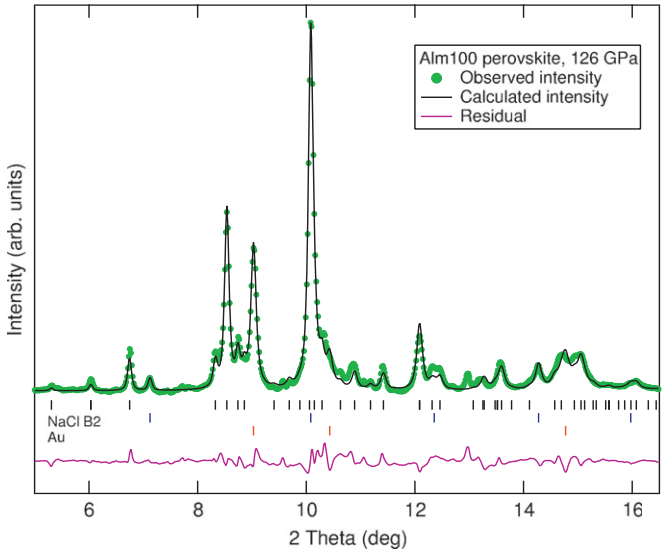

Fig. 3. Rietveld refinement results for orthorhombic $GdFeO_3$-type perovskite from Alm100 composition heated at 126 GPa. Data: green dots; fit: black line; residual: purple line; reference patterns for orthorhombic $GdFeO_3$-type perovskite, NaCl B2 phase and Au: sticks. Lattice parameters for perovskite phase are $a=4.387(2)$ Å, $b=4.605(2)$ Å, $c=6.353(2)$ Å, and $V=128.34(16)$ Å^3. (For interpretation of the references to color in this figure caption, the reader is referred to the web version of this article.)

Table 1
Atomic positions of almandine-composition perovskite at 126 GPa. Lattice parameters at this pressure are $a=4.387(2)$ Å, $b=4.605(2)$ Å, $c=6.353(2)$ Å, and $V=128.34(16)$ Å^3.

Site	Occupancy	x	y	z
A	75% Fe, 25% Al	0.5461 (13)	0.5687 (11)	0.25
B	75% Si, 25% Al	0.5	0	0.5
O1	O	0.141 (4)	0.469 (5)	0.25
O2	O	0.1523 (35)	0.2122 (33)	0.5460 (25)

perovskite in our experiment and also indicates that there are no major compositional gradients induced by laser heating. The recovery of garnet with no other detectable phases suggests that the synthesis of perovskite was not accompanied by significant oxidation of Fe^{2+} to ferric iron as this would make it more difficult to resynthesize a single-phase garnet composition. We also find no evidence in any of these compositions of Fe_2O_3 or metallic Fe that would be a signature of a disproportionation reaction during perovskite synthesis (Fialin et al., 2008; Frost et al., 2004; Lauterbach et al., 2000; Miyajima et al., 1999).

A separate Alm54 sample was directly decompressed from 84 GPa to ambient pressure without heating. The diffraction pattern of the recovered sample in this case contains several new peaks and could not be indexed as orthorhombic perovskite (Supplementary Fig. 3). Some of the observed d-spacings are consistent with a transformation to a $LiNbO_3$-type rhombohedral perovskite as previously reported for Pyr–Alm compositions (Funamori et al., 1997; Kesson et al., 1995), but not all observed diffraction peaks can be indexed to this phase. An Alm100 sample that was synthesized at 90 GPa and decompressed to 5 GPa retained the orthorhombic perovskite structure to this pressure. After the sample was removed from the diamond cell and examined at ambient conditions, new peaks appeared and the perovskite peaks were lost (Supplementary Fig. 3). This indicates that almandine-composition perovskite is not quenchable to ambient conditions.

All compositions were decompressed from the synthesis pressure at 5–10 GPa steps with heating to 2000–2500 K to relax differential stresses. At pressures between 59–71 GPa, $CaCl_2$-type SiO_2 diffraction peaks appeared in all compositions. The appearance of this phase was taken to indicate decomposition of perovskite to perovskite plus oxides. Due to peak overlap, magnesiowüstite peaks could not be identified. For single-phase Alm90-perovskite, heating at 56–61 GPa and 2000 K resulted in the appearance of the $CaCl_2$-type SiO_2 (110) diffraction peak (Fig. 2). The Alm100 perovskite partially decomposed to perovskite plus SiO_2 at 71 GPa after decompression from a synthesis pressure of 90 GPa. SiO_2 peaks appeared at lower pressures for low Fe contents. The pressure required to stabilize single-phase perovskite in highly Fe-rich compositions (Alm90–100) is $\sim$30 GPa higher than that required to synthesize single-phase perovskite from a pyrope (Alm0) composition (Kubo and Akaogi, 2000; Walter et al., 2004). The effect of Fe on the stability of perovskite in the Pyr–Alm system thus appears to be analogous to that in the En–Fs (Al-free) system (Mao et al., 1997; Dorfman et al., in press).

Laser heating stability was dependent on the sample absorption properties. The perovskite transition in Fe-rich silicates is known to induce a color change from transparent to black (O'Neill and Jeanloz, 1994; Kesson et al., 1995). This color change enhances coupling of the laser with the sample, resulting in a rapid spike in laser coupling during transformation. In runs where Alm38 and Alm73 were transformed at 76 and 77 GPa, respectively, this increase in laser coupling was observed visually as a flash, and peak temperatures may be well above the 2400–2800 K measured a few seconds later after the heating stabilized. In both of these samples, the diffraction pattern was textured and included peaks from both orthorhombic perovskite and Al_2O_3 (Fig. 1). Dissociation was also observed in an Alm100 sample heated to 3000 K at 91 GPa, to a highly textured mixture of perovskite and oxides SiO_2, FeO, and Al_2O_3. These observations suggest that at temperatures above 3000 K, almandine-composition perovskites may break down to a perovskite plus oxide mixture, as has been reported from quench studies (Miyajima et al., 1999; Kesson et al., 1995). The exsolution of Al_2O_3 is surprising as high temperatures tend to stabilize higher Al content in perovskite at lower pressures in less Fe-rich samples (Miyajima et al., 1999; Kubo and Akaogi, 2000). Alternatively, the phase mixture may have crystallized from brief melting during the runaway heating at 3000–4000 K (Knittle and Jeanloz, 1989). Heating was more stable in experiments on Alm54, Alm90, and Alm100 compositions as we were more successful controlling heating by immediately lowering the laser power at the phase transition.

Calculations for almandine at 1800 K and 0–100 GPa using the thermodynamic simulation software *HeFESTo* (Stixrude and Lithgow-Bertelloni, 2005, 2011; Xu et al., 2008) produce a sequence of phase transitions (Supplementary Fig. 4) in good agreement with our experimental data (L. Stixrude, pers. communication). At 24 GPa almandine garnet is predicted to break down to constituent oxides Al_2O_3, SiO_2, and FeO. At 40 GPa, Al_2O_3 and some SiO_2 and FeO react to form the perovskite phase. With increasing pressure, the oxides increasingly dissolve into the perovskite phase. Single-phase almandine-composition perovskite is predicted to be stable above 76 GPa. At higher temperature, the perovskite again coexists with oxides. No other phases are predicted that correspond to the unknown peaks we observed near 27 GPa. With this exception, all of these predictions match our observed phase assemblages and transition pressures for the Alm100 sample.

The thermodynamic parameters used in *HeFESTo* are not consistent with stability of single-phase perovskite in a pyrope ($Mg_3Al_2Si_3O_{12}$) composition at lower mantle conditions. Instead,

this composition is predicted to form a mixture of perovskite, SiO_2, and calcium-ferrite-type (cf) $MgAl_2O_4$ (Stixrude and Lithgow-Bertelloni, 2011). We did not observe the cf phase in diffraction patterns for any of the Pyr–Alm compositions we studied, nor has it been seen in previous experiments on the pyrope end-member up to 83 GPa (Kubo and Akaogi, 2000; Tateno et al., 2005; Walter et al., 2004). For an Alm50 composition, the cf phase is predicted by *HeFESTo* to be stable above 88 GPa, but below this pressure a single-phase perovskite is seen as in our Alm54 composition. Unlike almandine, the intermediate composition is predicted by the simulation to transform from garnet structure to a 4-phase mixture of perovskite, Al_2O_3, SiO_2, and (Mg,Fe)O at 29 GPa. The SiO_2 and (Mg,Fe)O components are predicted to fully dissolve into perovskite phase by 39 GPa, while the Al_2O_3 phase persists to 53 GPa. Our experiments produced SiO_2 at higher pressures in the Alm54 composition. However, this predicted lower solubility of the Al_2O_3 component could explain our observation of Al_2O_3 at 76–77 GPa in Alm38 and Alm73.

Fig. 4 shows a schematic phase diagram for Pyr–Alm compositions compiled from our experimental phase equilibrium data and previous work (Akaogi et al., 1998; Tateno et al., 2005; Shieh et al., 2011). Variation in transition pressures may be due in part to temperature differences; the data here represent samples quenched from laser heating to 1500–2600 K, and the synthesis temperature may have a significant effect on the phase assemblage and/or reaction kinetics. The solubility of Fe in perovskite increases with pressure as in the En–Fs system (Dorfman et al., in press). Above ~70 GPa it is possible to synthesize pure orthorhombic perovskite from more Fe-rich compositions than had been previously suggested (Kesson et al., 1995).

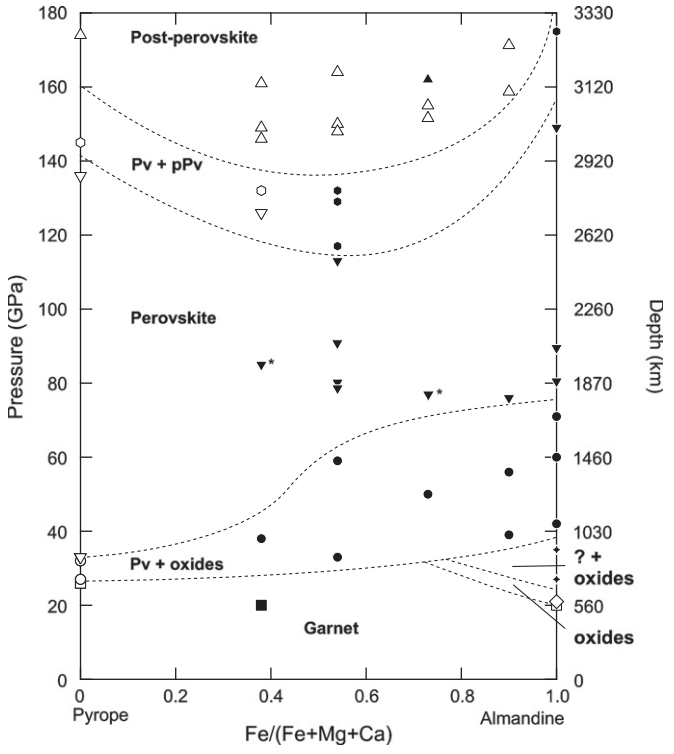

Fig. 4. Phase diagram for the pyr–alm compositions up to 180 GPa and ~2000 K. Phases observed in this (filled symbols) and previous studies (Irifune et al., 1996; Akaogi et al., 1998; Tateno et al., 2005; Shieh et al., 2011) (open symbols) are plotted as follows: post-perovskite, up-triangles; perovskite plus post-perovskite, hexagons; perovskite, down-triangles; perovskite plus oxides, circles; oxides plus unknown phase, stars; oxides, diamonds; garnet, squares. Starred perovskite observations included oxide phases perhaps due to unstable heating. Possible phase boundaries are shown as dashed curves. Curvature of perovskite plus oxides to perovskite phase boundary is suggested based on the Al-free system (Dorfman et al., in press).

2.3. Perovskite/post-perovskite phase transition

We also explored the perovskite-post-perovskite phase transition in the pyrope-almandine system. Alm73 and Alm100 were compressed to above 100 GPa and heated. Conversion of Pyr–Alm compositions to post-perovskites has been carried out for Alm0–Alm90 compositions at pressures 117 GPa and above (Tateno et al., 2005; Shieh et al., 2011), and our data provide additional constraints on the pressure-temperature boundaries of the perovskite-post-perovskite binary region.

As in previous work, heating Alm73 to 2000 K for 60 min at 163 GPa produced the post-perovskite phase with no evidence of perovskite peaks (Fig. 5). However, single-phase post-perovskite could not be synthesized for the Alm100 composition. Heating Alm100-perovskite to 2500–3000 K for an hour at pressures up to 149 GPa produced only perovskite with no observable post-perovskite peaks either during heating or after quench. This pressure is slightly higher than the 144–146 GPa pressures at which the coexistence of perovskite and post-perovskite was observed for the pyrope end-member composition (Tateno et al., 2005). At 177 GPa, heating Alm100-perovskite to 2300–2600 K for 60 min produced a mixture of perovskite and post-perovskite (Fig. 5). Further work is needed to determine whether single-phase Alm100 post-perovskite can be synthesized at higher pressures.

For intermediate Pyr–Alm compositions, Alm38 and Alm54, perovskite–post-perovskite mixtures were previously observed at 134 and 117 GPa, respectively (Shieh et al., 2011). These data suggest that Fe stabilizes post-perovskite relative to perovskite in Al-rich compositions as in Al-free compositions (Dorfman et al., in press). Limited observations have been made for compositions above ~ Fe# 50, but the stability of Alm100 perovskite at 149 GPa indicates an increase in the post-perovskite transition pressure. In Fig. 4, the post-perovskite transition in the Pyr–Alm

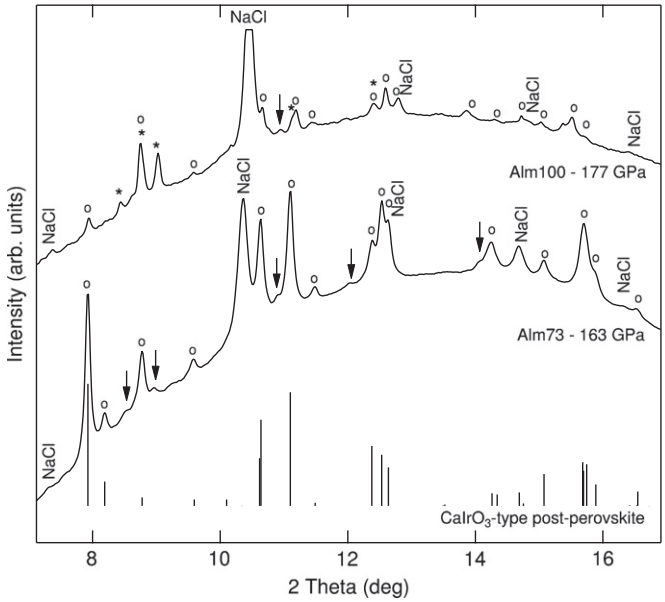

Fig. 5. Diffraction patterns ($\lambda = 0.3344$ Å) for Alm73 and Alm100 compositions after heating to 2000–2500 K for 60 min at 163 and 177 GPa, respectively. Alm73 can be indexed to $CaIrO_3$-type post-perovskite reference pattern with $a = 2.449(1)$ Å, $b = 7.999(2)$ Å, $c = 6.077(1)$ Å, and $V = 119.05(11)$ Å^3. Five minor unidentified peaks (arrows) do not match hcp-Fe, α-PbO_2-type or baddeleyite-type SiO_2, or $GdFeO_3$-type perovskite. Alm100 composition shows a mixture of perovskite (asterisks) and post-perovskite peaks (circles).

system is shown as a binary minimum, unlike the post-perovskite eutectoid or peritectoid predicted for the En–Fs system (Stixrude and Lithgow-Bertelloni, 2011). A two post-perovskite mixture was observed in some experiments by Shieh et al. (2011), and could account for additional complexity in this system.

2.4. Equation of state

Perovskites synthesized at 70–90 GPa were both compressed and decompressed at 5–10 GPa increments covering the range from 42 to 149 GPa. As discussed above, the Alm100 sample was further decompressed from 42 GPa directly to 5 GPa and the perovskite structure was retained. Volume compression data at 300 K are shown in Fig. 6. Samples were annealed at each pressure step by laser heating, typically at 1500–2000 K for 15 min. Anomalously high unit-cell volumes may indicate the presence of deviatoric stress in the sample (*e.g.* Duffy et al., 1999).

Deviatoric stresses can be generated in powder samples in the diamond anvil cell during cold compression (or decompression) as a result of local heterogeneities in the stress state associated with grain boundaries of differing orientations, elastic anisotropy, and non-hydrostatic stresses supported by the sample or pressure medium. Stress gradients and randomly distributed local deviatoric stresses broaden diffraction peaks to a degree corresponding to the distribution of longitudinal strain in the diffraction direction (Takemura, 2001; Weidner et al., 1994). Gold, due to its high elastic anisotropy, is a sensitive indicator of deviatoric stress (Duffy et al., 1999; Meng et al., 1993; Takemura and Dewaele, 2008). We evaluated the effectiveness of annealing in reducing deviatoric stresses in the mixed silicate and gold powder foil by comparing diffraction peak widths in gold to analogous measurements obtained under known quasi-hydrostatic conditions.

Laser annealing reduced diffraction peak full width at half maximum (FWHM) by as much as 25–60%. The resulting peak widths are comparable to previous measurements obtained in a He pressure medium (Takemura and Dewaele, 2008) (Supplementary Fig. 5) which is known to support minimal differential stress. We also observed that broader Au peaks correlated with higher measured perovskite volumes. The volume change upon annealing was due mostly to change in the *a* and *b* parameters. The *a* parameter is evidently the most sensitive to differential stress in Alm54 perovskite (Fig. 7). Alm100 samples loaded in Ne exhibited smaller volume and *b* lattice parameter above 100 GPa than samples loaded in NaCl. Ne is a more effective quasi-hydrostatic medium (Angel et al., 2007), and heating for 15 min

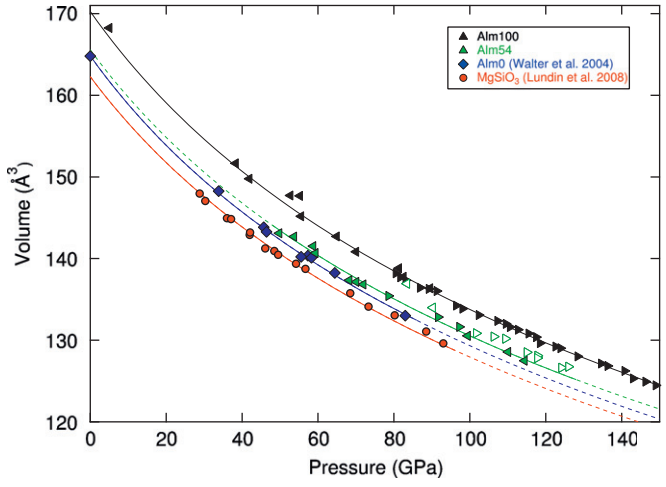

Fig. 6. Compression (right-pointing triangles) and decompression (left-pointing triangles) data for selected perovskite compositions. Data not used to fit equation of state due to differential stress are shown in open symbols. Solid lines are fits to the Birch–Murnaghan equation of state.

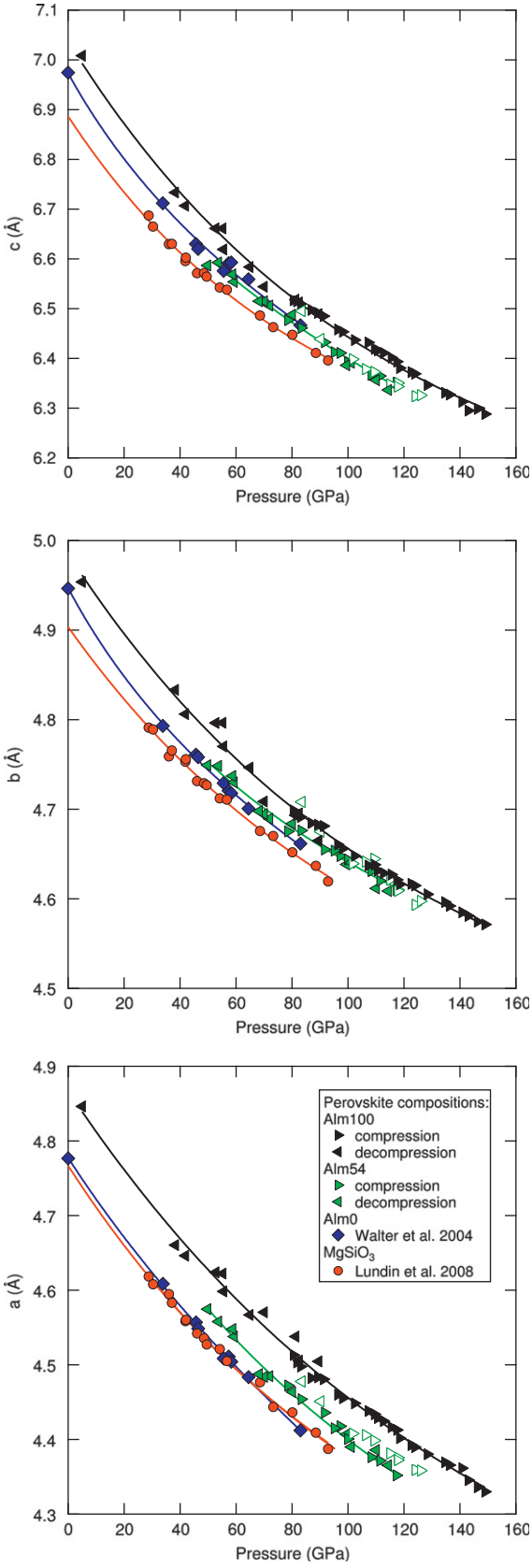

Fig. 7. Lattice parameters of perovskites up to 150 GPa. For Alm54, open symbols show data collected without annealing.

may not be enough to completely eliminate differential stress for samples in a NaCl medium. Volume data associated with anomalously high a or b parameters were not included in the equation of state fits.

Unit cell volumes were fit to the Birch–Murnaghan equation of state (Fig. 6). Fitting parameter results are given in Table 2. The zero-pressure bulk moduli, K_0, of Alm54- and Alm100-perovskites are similar, in the range of 252–261 GPa. These values are also not significantly different from observations for Al-free and low-Fe (Mg, Fe)SiO_3 perovskite (Lundin et al., 2008). The zero-pressure volume, V_0, obtained from Birch–Murnaghan fit of Alm100-perovskite is 5% larger than V_0 for $MgSiO_3$ perovskite. This corresponds to a 2% increase in zero-pressure density. As the density of $MgSiO_3$ perovskite is comparable to pyrope-composition perovskite, the density difference is due almost entirely to the FeO component.

The evolution of the lattice parameters of these perovskites (Fig. 7) shows the differing effects of Fe and Al on the perovskite structure. Previous studies have shown that the effect of substituting up to 25% trivalent cations Al or Fe^{3+} is to increase the b and c parameters but produce no significant change in a, overall increasing the anisotropy of the perovskite (Catalli et al., 2010; Walter et al., 2004). Substituting up to 15% Fe^{2+} has the opposite effect; the greatest expansion is in a, c may decrease slightly, and b is unchanged, resulting in decreased anisotropy (Lundin et al., 2008).

In the Pyr–Alm system, we observe lattice parameter compressibilities largely consistent with previously reported effects of Fe^{2+} and Al (Fig. 7). Increasing Fe-content has the strongest effect on the a parameter. The a cell parameter of the Alm100-composition perovskite is about 2% larger than the a parameter of Fe-free perovskites. The a parameter of Alm54-perovskite showed an intermediate 1% increase relative to Fe-free perovskite. These data are consistent with no effect of Al and a linear effect of Fe^{2+} on a. However, the b and c parameters vary nonlinearly with Fe-content. The b and c parameters for Alm54 perovskite are similar to values observed for the pyrope end-member (Walter et al., 2004), though c may be slightly smaller and b may be less compressible. This similarity agrees with previous findings (Walter et al., 2004; Lundin et al., 2008) that Al has a stronger effect on the b and c axes than Fe^{2+} and that the presence of Fe^{2+} results in a small contraction in c. Unlike less Fe-rich perovskites, Alm100-perovskite has significantly larger b and c parameters than $MgSiO_3$ perovskite. At 80 GPa, the Al in $(Mg_{0.75}Al_{0.25})(Al_{0.25}Si_{0.75})O_3$ perovskite increases c by 0.6% relative to $MgSiO_3$. The Fe in $(Fe_{0.75}Al_{0.25})(Al_{0.25}Si_{0.75})O_3$ perovskite doubles that to a 1.2% increase in c. This indicates either that there is a critical concentration of Fe above which increasing a alone cannot expand the unit cell enough to accommodate the larger Fe ion, or that some of the Fe in Alm100-composition perovskite is Fe^{3+}.

Table 2
Birch–Murnaghan equation of state fit parameters for perovskites with varying Fe and Al content. Uncertainties from fits with fixed K_0' from this work are obtained by varying K_0' from 3.5 to 4.5.

Composition	Pressure scale	V_0 (Å^3)	K_0 (GPa)	K_0'	K_{80} (GPa)
Alm100	Au	170.4 (0.9)	256 (13)	3.96 (0.14)	545
Alm100	Au	170.6 (1.0)	252 (30)	4[a]	543
Alm54	Au	165.6 (2.1)	261 (40)	4[a]	553
$MgSiO_3$[b]	Au	162.3	255–261 (1)	4[a]	544
$(Mg_{0.85}Fe_{0.15})SiO_3$[b]	Au	163.3	257–259 (1)	4[a]	549
$MgSiO_3$[c]	KBr	162.47	267.3 (6.9)	4[a]	575
Alm0 (pyrope)[c]	KBr	164.85	253.4 (6.2)	4[a]	545

K_{80}: the bulk modulus evaluated at 80 GPa.
[a] Parameter fixed during fit.
[b] Lundin et al. (2008), pressure given by Dewaele et al. (2004), Tsuchiya (2003).
[c] Walter et al. (2004).

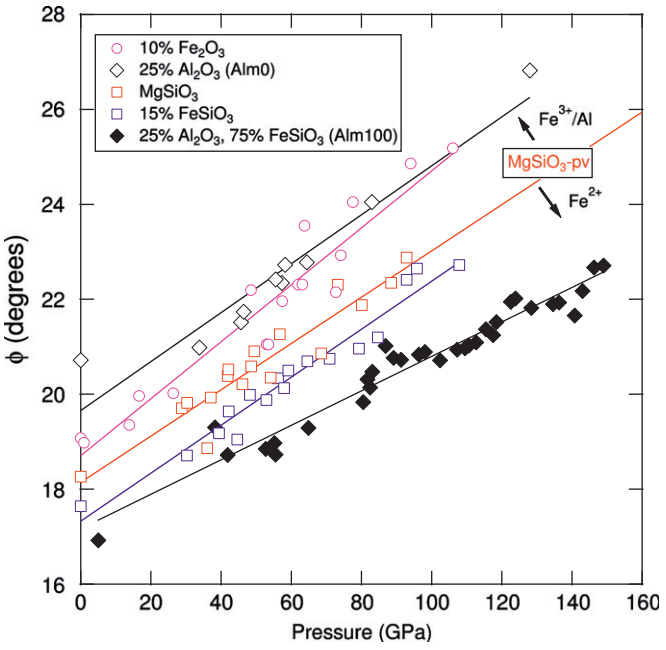

Fig. 8. Variation of the octahedral tilting angle (ϕ) of perovskite with pressure and composition. Data from previous work: pyrope (Alm0) composition from Walter et al. (2004), (Mg,Fe)SiO_3 from Lundin et al. (2008), (Mg,Fe)(Fe,Si)O_3 from Catalli et al. (2010).

Perovskite lattice parameter ratios can also clarify the effects of cation substitution on structure and anisotropy. Changes to the perovskite unit cell can be approximated as rotation of the SiO_6 octahedra (O'Keeffe et al., 1979). The octahedral tilting angle, ϕ, reflects the deviation from the ideal cubic perovskite structure ($\phi = 0$). We compute ϕ from the orthorhombic lattice parameters using the following equation (O'Keeffe et al., 1979):

$$\phi = \cos^{-1}\left(\frac{\sqrt{2}a^2}{bc}\right). \quad (1)$$

In silicate perovskites (Fig. 8), this parameter varies systematically with pressure and cation substitution. According to previous observations (Walter et al., 2004; Lundin et al., 2008; Catalli et al., 2010), pressure and substitution of trivalent cations Fe^{3+} and Al increase the tilting of the silica octahedra, whereas substitution of divalent Fe^{2+} decreases ϕ. Our almandine composition data follow this trend as well: ϕ is lower than all other compositions shown in Fig. 8 due to its high Fe^{2+} content, but not much lower due to the effect of Al. If the effect of Fe^{2+} on ϕ is linear, the difference in ϕ between the pyrope and almandine compositions is consistent with the replacement of the 75% Mg in the A-site with 75% Fe^{2+} and not with Fe^{3+}. The different mechanisms of divalent and trivalent cation substitution have opposite effects on perovskite anisotropy despite no significant effects on the bulk modulus.

4. Summary

Along the Pyr–Alm, $(Mg, Fe)_3Al_2Si_3O_{12}$, join from Alm38 to Alm100, we find that single-phase perovskites can be synthesized from garnet starting materials at 70–90 GPa and 2000–2500 K, corresponding to deep lower mantle pressure/temperature conditions. The end-member almandine-composition perovskite is

stable to at least 149 GPa. At 40–71 GPa, garnet compositions transformed to a mixture of perovskite and oxides, as evidenced by peaks of stishovite/$CaCl_2$-type SiO_2. The pressure required to form single-phase perovskite in this system increases with Fe-content. Additional work is needed to further constrain the compositional dependence of the P–T conditions of perovskite stability. The garnet-perovskite transition is reversible with heating, and orthorhombic perovskite cannot be quenched to ambient conditions but a rhombohedral phase appears to be formed upon quench to 1 bar.

Volume data for the Alm54 and Alm100 compositions were fit to the Birch–Murnaghan equation of state. These compositions represent the most Al-rich and Fe-rich perovskites measured to date. Despite large compositional differences, there is no significant difference between the compressibilities of these Fe- and Al-enriched silicate perovskites and $MgSiO_3$ perovskite. The calculated density of Alm100 perovskites is greater than that of $MgSiO_3$ perovskite by 18% at 80 GPa due to the presence of Fe.

Although no discontinuities were observed in the equation of state of these perovskites, a spin transition in Fe-bearing perovskite could be gradual or could have too small an effect on unit cell volume to be detectable by diffraction. Further analysis of these materials by synchrotron Mössbauer spectroscopy or X-ray emission spectroscopy could confirm the valence and spin state of Fe in these highly Fe-rich compositions.

Acknowledgments

This work was supported by the NSF and the Carnegie-DOE alliance center. We thank Z. Mao and J. Wang for their experimental assistance. L. Stixrude provided phase equilibria and seismic properties of pyrope, almandine and intermediate compositions simulated with the *HeFESTo* software. A. Hofmeister and H. O'Neill kindly provided natural and synthetic garnet samples. Diffraction analysis of starting materials was carried out at the PRISM Imaging and Analysis Center which is supported in part by the NSF MRSEC program through the Princeton Center for Complex Materials (Grant DMR-0819860). We thank E.E. Alp and L. Gao for assistance with Mössbauer spectroscopy of starting materials. Conventional Mössbauer spectroscopy at the Advanced Photon Source (APS), Argonne National Laboratory is supported by the Consortium for Materials Properties Research in Earth Sciences (COMPRES). High-pressure gas loading was supported by COMPRES and GeoSoilEnviroCARS. P. Dera, I. Kantor, A. Kubo, B. Lavina, S. Tkachev, and K. Zhuravlev assisted with beamline operations. Experiments were performed at GeoSoilEnviroCARS (Sector 13) and High Pressure Collaborative Access Team (HPCAT, Sector 16) at the APS. GeoSoil EnviroCARS is supported by the NSF - Earth Sciences (EAR-1128799) and DOE - Geosciences (DE-FG02-94ER14466). HPCAT is supported by CIW, CDAC, UNLV and LLNL through funding from DOE-NNSA and DOE-BES, with partial instrumentation funding by NSF. Use of the APS was supported by the U.S. Department of Energy, Office of Basic Energy Sciences, under Contract No. DE-AC02-06CH11357.

Appendix A. Supplementary data

Supplementary data associated with this article can be found in the online version at http://dx.doi.org.10.1016/j.epsl.2012.09.024.

References

Akaogi, M., Ohmura, N., Suzuki, T., 1998. High-pressure dissociation of $Fe_3Al_2Si_3O_{12}$ garnet: phase boundary determined by phase equilibrium experiments and calorimetry. Phys. Earth Planet. Inter. 106 (March (1–2)), 103–113.

Akber-Knutson, S., Steinle-Neumann, G., Asimow, P.D., 2005. Effect of Al on the sharpness of the $MgSiO_3$ perovskite to post-perovskite phase transition. Geophys. Res. Lett. 32 (July), L14303.

Andrault, D., 2001. Evaluation of (Mg, Fe) partitioning between silicate perovskite and magnesiowüstite up to 120 GPa and 2300 K. J. Geophys. Res. 106 (B2), 2079–2087.

Andrault, D., Bolfan-Casanova, N., Bouhifd, M.A., Guignot, N., Kawamoto, T., 2007. The role of Al-defects on the equation of state of Al-(Mg, Fe)SiO_3 perovskite. Earth Planet. Sci. Lett. 263 (November (3–4)), 167–179.

Andrault, D., Bolfan-Casanova, N., Guignot, N., 2001. Equation of state of lower mantle (Al, Fe)-$MgSiO_3$ perovskite. Earth Planet. Sci. Lett. 193 (December (3–4)), 501–508.

Angel, R.J., Bujak, M., Zhao, J., Gatta, G.D., Jacobsen, S.D., 2007. Effective hydrostatic limits of pressure media for high-pressure crystallographic studies. J. Appl. Crystallogr. 40 (1), 26–32.

Boffa Ballaran, T., Kurnosov, A., Glazyrin, K., Frost, D.J., Merlini, M., Hanfland, M., Caracas, R., 2012. Effect of chemistry on the compressibility of silicate perovskite in the lower mantle. Earth Planet. Sci. Lett. 333–334 (June), 181–190.

Caracas, R., Cohen, R., 2008. Ferrous iron in post-perovskite from first-principles calculations. Phys. Earth Planet. Inter. 168 (July (3–4)), 147–152.

Catalli, K., Shim, S.-H., Dera, P., Prakapenka, V.B., Zhao, J., Sturhahn, W., Chow, P., Xiao, Y., Cynn, H., Evans, W.J., 2011. Effects of the Fe^{3+} spin transition on the properties of aluminous perovskite and new insights for lower-mantle seismic heterogeneities. Earth Planet. Sci. Lett. 310 (October(3–4)), 293–302.

Catalli, K., Shim, S.-H., Prakapenka, V.B., Zhao, J., Sturhahn, W., Chow, P., Xiao, Y., Liu, H., Cynn, H., Evans, W.J., 2010. Spin state of ferric iron in $MgSiO_3$ perovskite and its effect on elastic properties. Earth Planet. Sci. Lett. 289 (January (1–2)), 68–75.

Conrad, P.G., Shen, G., Mao, H.-k., Fei, Y., Hemley, R.J., 1996. Stability of garnets in the system $MgSiO_3$–$FeSiO_3$–Al_2O_3 at high pressure. In: US–Japan Seminar High Pressure-Temperature Research: Properties of Earth and Planetary Materials, vol. 73.

Daniel, I., Bass, J.D., Fiquet, G., Cardon, H., Zhang, J., 2004. Effect of aluminium on the compressibility of silicate perovskite. Geophys. Res. Lett. 31, L15608.

Daniel, I., Cardon, H., Fiquet, G., Guyot, F., Mezouar, M., 2001. Equation of state of Al-bearing perovskite to lower mantle pressure conditions. Geophys. Res. Lett 28 (19), 3789–3792.

Dewaele, A., Loubeyre, P., Mezouar, M., 2004. Equations of state of six metals above 94 GPa. Phys. Rev. B (Cond. Matter Mater. Phys.) 70 (9), 94112.

Dorfman, S.M., Meng, Y., Prakpenka, V.B., Duffy, T.S. Effects of Fe-enrichment on the equation of state and stability of (Mg, Fe)SiO_3 perovskite and post-perovskite, Earth and Planetary Science Letters, in press.

Duffy, T.S., Shen, G., Heinz, D.L., Shu, J., Ma, Y., Mao, H.-k., Hemley, R.J., Singh, A.K., 1999. Lattice strains in gold and rhenium under nonhydrostatic compression to 37 GPa. Phys. Rev. B (Cond. Matter Mater. Phys.) 60 (December (22)), 15063–15073.

Fei, Y., 1998. Solid solutions and element partitioning at high pressures and temperatures. Rev. Mineral. Geochem. 37 (January (1)), 343–367.

Fei, Y., Ricolleau, A., Frank, M., Mibe, K., Shen, G., Prakapenka, V.B., 2007. Toward an internally consistent pressure scale. Proceedings of the National Academy of Sciences 104 (May (22)), 9182–9186.

Fei, Y., Wang, Y., Finger, L.W., 1996. Maximum solubility of FeO in (Mg, Fe)SiO_3-perovskite as a function of temperature at 26 GPa: implication for FeO content in the lower mantle. J. Geophys. Res. 101 (B5), 11525–11530.

Fialin, M., Catillon, G., Andrault, D., 2008. Disproportionation of Fe^{2+} in Al-free silicate perovskite in the laser heated diamond anvil cell as recorded by electron probe microanalysis of oxygen. Phys. Chem. Miner. 36 (4), 183–191.

Frost, D.J., Langenhorst, F., 2002. The effect of Al_2O_3 on Fe–Mg partitioning between magnesiowüstite and magnesium silicate perovskite. Earth Planet. Sci. Lett. 199 (May (1–2)), 227–241.

Frost, D.J., Liebske, C., Langenhorst, F., McCammon, C.A., Trønnes, R.G., Rubie, D.C., 2004. Experimental evidence for the existence of iron-rich metal in the Earth's lower mantle. Nature 428 (6981), 409–412.

Fujino, K., Nishio-Hamane, D., Seto, Y., Sata, N., Nagai, T., Shinmei, T., Irifune, T., Ishii, H., Hiraoka, N., Cai, Y.Q., Tsuei, K., 2012. Spin transition of ferric iron in Al-bearing Mg-perovskite up to 200 GPa and its implication for the lower mantle. Earth Planet. Sci. Lett. 317–318 (February), 407–412.

Fujino, K., Nishio-Hamane, D., Suzuki, K., Izumi, H., Seto, Y., Nagai, T., 2009. Stability of the perovskite structure and possibility of the transition to the post-perovskite structure in $CaSiO_3$, $FeSiO_3$, $MnSiO_3$ and $CoSiO_3$. Phys. Earth Planet. Inter. 177 (3–4), 147–151.

Funamori, N., Yagi, T., Miyajima, N., Fujino, K., 1997. Transformation in garnet from orthorhombic perovskite to $LiNbO_3$ phase on release of pressure. Science 275 (January (5299)), 513–515.

Garnero, E.J., McNamara, A.K., 2008. Structure and dynamics of Earth's lower mantle. Science 320 (May (5876)), 626–628.

Hammersley, A.P., Svensson, S.O., Hanfland, M., Fitch, A.N., Hausermann, D., 1996. Two-dimensional detector software: from real detector to idealised image or two-theta scan. High Press. Res. 14, 235–248.

Hofmeister, A.M., 2006. Thermal diffusivity of garnets at high temperature. Phys. Chem. Miner. 33 (January (1)), 45–62.

Hofmeister, A.M., Schaal, R.B., Campbell, K.R., Berry, S.L., Fagan, T.J., 1998. Prevalence and origin of birefringence in 48 garnets from the pyrope-almandine-grossularite-spessartine quaternary. Am. Mineral. 83 (11–12 Part 1), 1293.

Holland, T.J.B., Redfern, S.A.T., 1997. Unit cell refinement from powder diffraction data: the use of regression diagnostics. Mineral. Mag. 61, 65–77.
Irifune, T., Koizumi, T., Ando, J., 1996. An experimental study of the garnet-perovskite transformation in the system $MgSiO_3$–$Mg_3Al_2Si_3O_{12}$. Phys. Earth Planet. Inter. 96 (August (2–3)), 147–157.
Ishii, M., Tromp, J., 2004. Constraining large-scale mantle heterogeneity using mantle and inner-core sensitive normal modes. Phys. Earth Planet. Inter. 146 (August (1–2)), 113–124.
Ito, E., Kubo, A., Katsura, T., Akaogi, M., Fujita, T., 1998. High-pressure transformation of pyrope ($Mg_3Al_2Si_3O_{12}$) in a sintered diamond cubic anvil assembly. Geophys. Res. Lett. 25 (6), 821–824.
Kesson, S.E., Fitzgerald, J.D., Shelley, J.M.G., Withers, R.L., 1995. Phase relations, structure and crystal chemistry of some aluminous silicate perovskites. Earth Planet. Sci. Lett. 134 (August (1–2)), 187–201.
Knittle, E., Jeanloz, R., 1987. Synthesis and equation of state of (Mg, Fe)SiO_3 perovskite to over 100 gigapascals. Science 235 (4789), 668–670.
Knittle, E., Jeanloz, R., 1989. Melting curve of (Mg, Fe)SiO_3 perovskite to 96 GPa: evidence for a structural transition in lower mantle melts. Geophys. Res. Lett. 16 (5), 421–424.
Kubo, A., Akaogi, M., 2000. Post-garnet transitions in the system $Mg_4Si_4O_{12}$–$Mg_3Al_2Si_3O_{12}$ up to 28 GPa: phase relations of garnet, ilmenite and perovskite. Phys. Earth Planet. Inter. 121 (September (1–2)), 85–102.
Larson, A.C., Von Dreele, R.B., 2000. General Structure Analysis System (GSAS). Los Alamos National Laboratory Report LAUR, pp. 86–748.
Lauterbach, S., McCammon, C.A., van Aken, P., Langenhorst, F., Seifert, F., 2000. Mössbauer and ELNES spectroscopy of (Mg, Fe)(Si,Al)O_3 perovskite: a highly oxidised component of the lower mantle. Contrib. Mineral. Petrol. 138 (January (1)), 17–26.
Lee, C.A., Luffi, P., Hoink, T., Li, J., Dasgupta, R., Hernlund, J., 2010. Upside-down differentiation and generation of a 'primordial' lower mantle. Nature 463 (February (7283)), 930–933.
Liu, L., 1974. Silicate perovskite from phase transformations of pyrope-garnet at high pressure and temperature. Geophys. Res. Lett. 1 (6), 277–280.
Lundin, S., Catalli, K., Santillan, J., Shim, S.-H., Prakapenka, V.B., Kunz, M., Meng, Y., 2008. Effect of Fe on the equation of state of mantle silicate perovskite over 1 Mbar. Phys. Earth Planet. Inter. 168 (May (1–2)), 97–102.
Mao, H.-k., Hemley, R.J., Fei, Y., Shu, J.F., Chen, L.C., Jephcoat, A.P., Wu, Y., Bassett, W.A., 1991. Effect of pressure, temperature, and composition on lattice parameters and density of (Fe, Mg)SiO_3-perovskites to 30 GPa. J. Geophys. Res. 96 (B5), 8069–8079.
Mao, H.-k., Shen, G., Hemley, R.J., 1997. Multivariable dependence of Fe–Mg partitioning in the lower mantle. Science 278 (5346), 2098–2100.
Mao, W.L., Mao, H.-k., Sturhahn, W., Zhao, J., Prakapenka, V.B., Meng, Y., Shu, J., Fei, Y., Hemley, R.J., 2006. Iron-rich post-perovskite and the origin of ultralow-velocity zones. Science 312 (April (5773)), 564–565.
Mao, W.L., Meng, Y., Shen, G., Prakapenka, V.B., Campbell, A.J., Heinz, D.L., Shu, J., Caracas, R., Cohen, R.E., Fei, Y., 2005. Iron-rich silicates in the Earth's D″ layer. Proc. Nat. Acad. Sci. 102 (28), 9751–9753.
Mao, W.L., Shen, G., Prakapenka, V.B., Meng, Y., Campbell, A.J., Heinz, D.L., Shu, J., Hemley, R.J., Mao, H.-k., 2004. Ferromagnesian postperovskite silicates in the D″ layer of the earth. Proc. Nat. Acad. Sci. US Am. 101 (November (45)), 15867–15869.
Mao, Z., Lin, J., Scott, H., Watson, H., Prakapenka, V., Xiao, Y., Chow, P., McCammon, C., 2011. Iron-rich perovskite in the Earth's lower mantle. Earth Planet. Sci. Lett. 309 (September (3–4)), 179–184.
McNamara, A.K., Zhong, S., 2005. Thermochemical structures beneath Africa and the Pacific Ocean. Nature 437 (October (7062)), 1136–1139.
Meng, Y., Shen, G., Mao, H.-k., 2006. Double-sided laser heating system at HPCAT for in situ x-ray diffraction at high pressures and high temperatures. J. Phys.: Cond. Matter 18 (25), 1097.
Meng, Y., Weidner, D.J., Fei, Y., 1993. Deviatoric stress in a quasi-hydrostatic diamond anvil cell: effect on the volume-based pressure calibration. Geophys. Res. Lett. 20 (12), 1147–1150.
Ming, L., Bassett, W., 1975. Decomposition of $FeSiO_3$ into $FeO+SiO_2$ under very high pressure and high temperature. Earth Planet. Sci. Lett. 25 (1), 68–70.
Miyajima, N., Fujino, K., Funamori, N., Kondo, T., Yagi, T., 1999. Garnet-perovskite transformation under conditions of the Earth's lower mantle: an analytical transmission electron microscopy study. Phys. Earth Planet. Inter. 116 (December (1–4)), 117–131.
Murakami, M., Hirose, K., Kawamura, K., Sata, N., Ohishi, Y., 2004. Post-perovskite phase transition in $MgSiO_3$. Science 304 (5672), 855–858.
Nishio-Hamane, D., Fujino, K., Seto, Y., Nagai, T., 2007. Effect of the incorporation of $FeAlO_3$ into $MgSiO_3$ perovskite on the post-perovskite transition. Geophys. Res. Lett. 34, L12307.
Nishio-Hamane, D., Nagai, T., Fujino, K., Seto, Y., Takafuji, N., 2005. Fe^{3+} and Al solubilities in $MgSiO_3$ perovskite: implication of the Fe^{3+} and Al_2O_3 substitution in $MgSiO_3$ perovskite at the lower mantle condition. Geophys. Res. Lett. 32, L16306.
Nishio-Hamane, D., Seto, Y., Fujino, K., Nagai, T., 2008. Effect of $FeAlO_3$ incorporation into $MgSiO_3$ perovskite on the bulk modulus of perovskite. Phys. Earth Planet. Inter. 166 (February (3–4)), 219–225.
Oganov, A.R., Ono, S., 2004. Theoretical and experimental evidence for a post-perovskite phase of $MgSiO_3$ in Earth's D″ layer. Nature 430 (July (6998)), 445–448.
O'Keeffe, M., Hyde, B.G., Bovin, J., 1979. Contribution to the crystal chemistry of orthorhombic perovskites: $MgSiO_3$ and $NaMgF_3$. Phys. Chem. Miner. 4 (4), 299–305.
O'Neill, B., Jeanloz, R., 1994. $MgSiO_3$–$FeSiO_3$–Al_2O_3 in the Earth's lower mantle: perovskite and garnet at 1200 km depth. J. Geophys. Res. 99 (B10), 19901–19915.
Prakapenka, V.B., Kubo, A., Kuznetsov, A., Laskin, A., Shkurikhin, O., Dera, P., Rivers, M.L., Sutton, S.R., 2008. Advanced flat top laser heating system for high pressure research at GSECARS: application to the melting behavior of germanium. High Press. Res. 28 (September (3)), 225–235.
Ross, N., Hazen, R., 1990. High-pressure crystal chemistry of $MgSiO_3$ perovskite. Phys. Chem. Miner. 17 (June (3)), 228–237.
Saikia, A., Boffa Ballaran, T., Frost, D.J., 2009. The effect of Fe and Al substitution on the compressibility of $MgSiO_3$-perovskite determined through single-crystal X-ray diffraction. Phys. Earth Planet. Inter. 173 (March (1–2)), 153–161.
Shen, G., Rivers, M.L., Wang, Y., Sutton, S.R., 2001. Laser heated diamond cell system at the advanced photon source for in situ x-ray measurements at high pressure and temperature. Rev. Sci. Instrum. 72 (2), 1273.
Shieh, S.R., Dorfman, S.M., Kubo, A., Prakapenka, V.B., Duffy, T.S., 2011. Synthesis and equation of state of post-perovskites in the $(Mg, Fe)_3Al_2Si_3O12$ system. Earth Planet. Sci. Lett. 312 (December (3–4)), 422–428.
Shim, S.-H., 2008. The postperovskite transition. Annu. Rev. Earth Planet. Sci. 36 (May (1)), 569–599.
Stixrude, L., Lithgow-Bertelloni, C., 2005. Thermodynamics of mantle minerals I. physical properties. Geophys. J. Int. 162 (2), 610–632.
Stixrude, L., Lithgow-Bertelloni, C., 2011. Thermodynamics of the Earth's mantle – II. Phase equilbria. Rev. Mineral. Geochem. 71 (1), 465.
Takemura, K., 2001. Evaluation of the hydrostaticity of a helium-pressure medium with powder x-ray diffraction techniques. J. App. Phys. 89 (1), 662–668.
Takemura, K., Dewaele, A., 2008. Isothermal equation of state for gold with a He-pressure medium. Phys. Rev. B (Cond. Matter Mater. Phys.) 78 (10) 104119–13.
Tateno, S., Hirose, K., Sata, N., Ohishi, Y., 2005. Phase relations in $Mg_3Al_2Si_3O_{12}$ to 180 GPa: effect of Al on post-perovskite phase transition. Geophys. Res. Lett. 32, L15306.
Tateno, S., Hirose, K., Sata, N., Ohishi, Y., 2007. Solubility of FeO in (Mg, Fe)SiO_3 perovskite and the post-perovskite phase transition. Phys. Earth Planet. Inter. 160 (March (3–4)), 319–325.
Toby, B.H., 2001. EXPGUI, a graphical user interface for GSAS. J. Appl. Crystallogr. 34 (2), 210–213.
Trampert, J., Deschamps, F., Resovsky, J., Yuen, D., 2004. Probabilistic tomography maps chemical heterogeneities throughout the lower mantle. Science 306 (5697), 853.
Tsuchiya, J., Tsuchiya, T., 2008. Postperovskite phase equilibria in the $MgSiO_3$–Al_2O_3 system. Proc. Nat. Acad. Sci. 105 (December (49)), 19160–19164.
Tsuchiya, T., 2003. First-principles prediction of the P-V-T equation of state of gold and the 660-km discontinuity in Earth's mantle. J. Geophys. Res. 108 (October (2462)), 9.
Walter, M.J., Kubo, A., Yoshino, T., Brodholt, J., Koga, K.T., Ohishi, Y., 2004. Phase relations and equation-of-state of aluminous Mg-silicate perovskite and implications for Earth's lower mantle. Earth Planet. Sci. Lett. 222, 501–516.
Walter, M.J., Trønnes, R.G., Armstrong, L.S., Lord, O.T., Caldwell, W.A., Clark, S.M., 2006. Subsolidus phase relations and perovskite compressibility in the system MgO–$AlO_{1.5}$–SiO_2 with implications for Earth's lower mantle. Earth Planet. Sci. Lett. 248 (May (2)), 77–89.
Weidner, D.J., Wang, Y., Meng, Y., Vaughan, M.T., Jul. 1994. Deviatoric stress measurements at high pressure and temperature. AIP Conference Proceedings, vol. 309(1), pp. 1025–1028.
Williams, Q., Garnero, E.J., 1996. Seismic evidence for partial melt at the base of Earth's mantle. Science 273 (September (5281)), 1528–1530.
Xu, W., Lithgow-Bertelloni, C., Stixrude, L., Ritsema, J., 2008. The effect of bulk composition and temperature on mantle seismic structure. Earth Planet. Sci. Lett. 275 (1–2), 70–79.
Zhang, J., Weidner, D.J., 1999. Thermal equation of state of aluminum-enriched silicate perovskite. Science 284 (April (5415)), 782–784.